Exploring Quantum Phases of Dipolar Gases through Quasicrystalline Confinement

Vinicius Zampronio,[1,2,*] Alejandro Mendoza-Coto,[3,4,†] Tommaso Macrì,[5,1,‡] and Fabio Cinti[2,6,7,§]

[1]*Departamento de Física Teórica e Experimental, Universidade Federal do Rio Grande do Norte, 59075-000 Natal, Brazil*
[2]*Dipartimento di Fisica e Astronomia, Università di Firenze, I-50019 Sesto Fiorentino (FI), Italy*
[3]*Departamento de Física, Universidade Federal de Santa Catarina, 88040-900 Florianópolis, Brazil*
[4]*Max Planck Institute for the Physics of Complex Systems, Nöthnitzer strasse 38, 01187 Dresden, Germany*
[5]*ITAMP, Harvard-Smithsonian Center for Astrophysics, Cambridge, Massachusetts 02138, USA*
[6]*INFN, Sezione di Firenze, I-50019 Sesto Fiorentino (FI), Italy*
[7]*Department of Physics, University of Johannesburg, P.O. Box 524, Auckland Park 2006, South Africa*

(Received 12 March 2024; accepted 30 September 2024; published 6 November 2024)

The effects of frustration on extended supersolid states is a largely unexplored subject in the realm of cold-atom systems. In this work, we explore the impact of quasicrystalline lattices on the supersolid phases of dipolar bosons. Our findings reveal that weak quasicrystalline lattices can induce a variety of modulated phases, merging the inherent solid pattern with a quasiperiodic decoration induced by the external potential. As the lattice becomes stronger, we observe a superquasicrystal phase and a Bose glass phase. Our results, supported by a detailed discussion on experimental feasibility using dysprosium atoms and quasicrystalline optical lattice potentials, open a new avenue in the exploration of long-range interacting quantum systems in aperiodic environments. We provide a solid foundation for future experimental investigations, potentially confirming our theoretical predictions and contributing profoundly to the field of quantum gases in complex external potentials.

DOI: 10.1103/PhysRevLett.133.196001

Introduction—The exploration of exotic quantum phases displaying simultaneously different kinds of orders, or *quasi*-orders in systems with long-range interactions, has emerged as a central goal in condensed-matter physics [1]. Among these, electronic liquid crystals [2,3], Bose glasses (BGs) [4,5], supersolids [6–9], and quantum systems with quasiperiodic order [10–14] stand out as intriguing manifestations combining translational, rotational, and global gauge symmetry breaking. Such systems exhibit exotic collective behaviors arising from intricate interplays between quantum effects, topology, and interactions, holding promise for applications ranging from quantum simulators to advanced materials [9,15–21]. In this context, the study of dipolar bosons has garnered increasing interest, driven by advancements in both theoretical [22–34] and experimental [35–45] research.

Recent investigations in these systems revealed a rich phase diagram with three distinct supersolid phases—stripes, triangular, and honeycomb—eventually converging at a critical point [31,46,47]. In the conventional scenario, the crystallization transition is expected to be first-order, resulting in a sudden increase in the modulation amplitude upon dynamically crossing the crystallization line. This impacts the phase coherence of the system and leads to the generation of high-energy excitations [48], hindering the stability of the supersolid phase.

Exploring the introduction of disorder into these systems could further open new avenues for understanding pioneering complex phases. In noninteracting 2D models, disorder generates nontrivial effects such as Anderson localization (AL) [49–51]. Moreover, the presence of contact interactions in disordered Bose systems frustrates AL and leads to the emergence of BG physics [5,52] and many-body localization [53]. Quasicrystal lattices (QCLs) present intriguing platforms for investigating disorder-induced phenomena, particularly due to the observed phase transition from extended to exponentially localized states with increasing QCL intensity [5,50,54]. In QCL environments, quantum gases with contact interactions exhibit not only the anticipated disordered system effects [55–62], but also the emergence of quasicrystalline superfluids [11]. In the case of long-range interacting dipolar systems, an intriguing possibility is the study of frustrated phases resulting from the competition between the natural tendency of the system to form periodic supersolids and the presence of a QCL.

In this Letter, we bridge the physics of long-range dipolar bosons with the effects of QCL confinement. By numerically solving extensive Gross-Pitaevskii equations (GPEs), we explore the phase diagram of the model guided by a spectral variational study. We observe the emergence

*Contact author: v.zamproniopedroso@unifi.it
†Contact author: alejandro.mendoza@ufsc.br
‡Contact author: tommasomacri@gmail.com
§Contact author: fabio.cinti@unifi.it

of global-ordered phases, whose formation mechanism is triggered by the local disorder generated by the QCL. Importantly, our analysis guides experimental implementations within the scope of current technological capabilities. This approach offers the potential to probe and explore these intriguing phases of matter, significantly enhancing our understanding of quantum systems in complex potentials.

Model and methods—We consider a gas of N interacting bosons of mass m and dipolar length a_{dd} at $T = 0$. The atoms are harmonically trapped along the polarization axis and subjected to a QCL [56,57] in the plane perpendicular to the polarization axis. The condensate wave function, $\psi(\mathbf{r})$, is normalized to unity; hence the local atomic density is given by $\rho(\mathbf{r}) = N|\psi(\mathbf{r})|^2$. Choosing the units of length as $\ell = 12\pi a_{dd}$ and time as $t_0 = m\ell^2/\hbar$, we can express the GPE [63,64] as

$$i\frac{d\psi(\mathbf{r})}{dt} = \left[-\frac{1}{2}\nabla^2 + U(z) + U_q(\mathbf{r}) + \gamma N^{3/2}|\psi(\mathbf{r})|^3 + \frac{a_s}{3a_{dd}}N|\psi(\mathbf{r})|^2 + \frac{N}{4\pi}\int d\mathbf{r}' V(\mathbf{r}-\mathbf{r}')|\psi(\mathbf{r}')|^2\right]\psi(\mathbf{r}). \quad (1)$$

The first term on the right-hand side of Eq. (1) pertains to the kinetic energy, while the second term corresponds to the axial trapping potential $U(z) = \omega_z^2 z^2/2$, ω_z being the frequency of the axial trap. The in-plane octagonal QCL is described by $U_q(\mathbf{r}) = \sum_{i=0}^{3} U_0[1 - \cos(\mathbf{q}_i \cdot \mathbf{r})]/2$, with characteristic wave vectors $\mathbf{q}_i = q[\cos(i\pi/4), \sin(i\pi/4), 0]$ [65]. The fourth contribution to Eq. (1) corresponds to the Lee-Huang-Yang (LHY) correction to the mean-field approximation [66–68], where $\gamma = (4/3\pi^2)(a_s/3a_{dd})^{5/2}[1 + \frac{3}{2}(a_s/a_{dd})^2]$ [69,70]. Finally, the last two terms of Eq. (1) account for the scaled contact interaction, with scattering length a_s, and the dipolar interaction, $V(\mathbf{r}) = [1 - (3z^2/r^2)](1/r^3) + (8\pi/3)\delta(r)$. The ground state ψ_0 of the system is obtained by evolving an initial ansatz $\psi(\mathbf{r}, t = 0)$ in imaginary time. Details about $\psi(\mathbf{r}, t = 0)$ are described in the Supplemental Material [71].

We have also implemented a spectral variational method (SVM), see [71] and [13,31,72]. In summary, after introducing the average 2D density of particles $\rho_\perp(\mathbf{r}_\perp) = N\int dz|\psi_0|^2(\mathbf{r})$, an effective energy functional in terms of $\rho_\perp(\mathbf{r}_\perp) = N|\psi_\perp|^2(\mathbf{r}_\perp)$ is constructed and used to study the extended phases of the system [71]. The SVM shows that the optimal orientation of the periodic structure of the pattern with respect to one of the main directions of the QCL, is $\pi/8$. Such a configuration is challenging to implement in the GPE solution, considering the constraints imposed by the periodic boundary conditions. However, our analytical study shows that considering two main directions of the periodic pattern and the QCL, respectively, aligned, have a negligible energy cost, making numerical results with aligned patterns an excellent approximation of the actual ground state of the system [71].

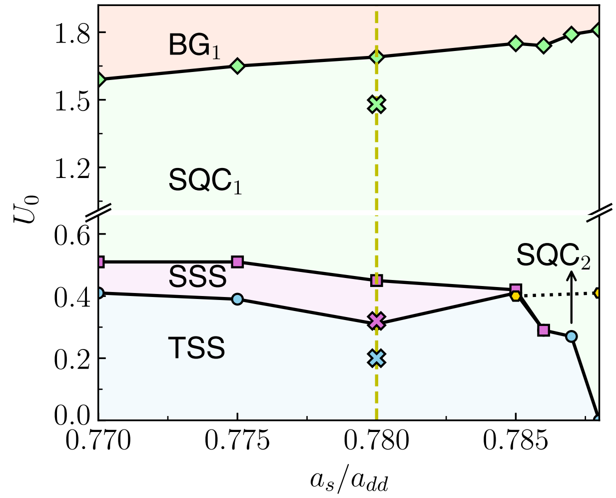

FIG. 1. Phase diagram of dipolar bosons in a quasicrystalline lattice. We numerically solve Eq. (1) in imaginary time to demonstrate the emergence of several phases induced by the simultaneous effect of a quasicrystalline potential with intensity U_0 and contact (with strength a_s) and dipolar (a_{dd}) interactions. We observe the triangular-supersolid (TSS), stripe-supersolid (SSS), superquasicrystal (SQC$_{i=1,2}$), and Bose glass (BG$_1$) phases, as described in the text. The average scaled density of the effective two-dimensional system is $\bar{\rho}_\perp = 120$, the wave vector of the QCL is $q = 1.8$, and the frequency of the harmonic trap along the polarization axis is $\omega_z = 0.08$. Solid lines delimit the phase boundaries. The dotted line guides the eye for the crossover between different SQC structures. The vertical dashed line corresponds to the analysis in Fig. 3. The crosses are representative points of the density patterns in Fig. 2.

Results—We numerically solve the GPE considering $\omega_z = 0.08$, average in-plane density $\bar{\rho}_\perp = 120$, and $0.77 \leq a_s/a_{dd} \lesssim 0.79$. The characteristic wave vectors of the QCL have moduli $q = 1.8$, which is about five times the characteristic wave vector k_0 of the triangular supersolid (TSS) found when $U_0 = 0$. As shown in the phase diagram in Fig. 1, which is constructed by tuning the QCL intensity U_0 and a_s/a_{dd}, we identify five distinct phases in the regime of parameters considered: a TSS; a stripe supersolid (SSS); superquasicrystal phases (SQC$_{i=1,2}$), where the quasicrystalline density pattern coexists with a finite superfluid fraction, and a Bose glass (BG$_{i=1}$). Interestingly, we observe a crossover between a quasicrystalline pattern matching the external lattice ($i = 2$) and a state in which it does not ($i = 1$). As an effect of the long-range repulsion, many lattice sites can be depleted, resulting in a density pattern skipping a significant fraction of the QCL minima, see Supplemental Material [71]. On the other hand, when a_s/a_{dd} is large, and U_0 is weak, the delocalization of the pattern is enhanced, and the system undergoes a crossover to a SQC state matching the QCL. The dotted line in

Fig. 1 is a guide to the eye for the crossover region separating the SQC_1 and SQC_2 states. It is obtained from an analysis of the local maxima structure in $\tilde{\psi}_\perp(\mathbf{k}_\perp) \propto \int d\mathbf{r}_\perp \psi_\perp(\mathbf{r}_\perp) e^{i\mathbf{k}_\perp \cdot \mathbf{r}_\perp}$. For this observable, two sets of local maxima can be identified, those located at $|\mathbf{k}_\perp| = q$, corresponding to Fourier modes matching the QCL and those located at $|\mathbf{k}_\perp| \neq q$, responsible for producing a quasicrystalline pattern not matching the QCL. The position of the dotted line defines the moment when the sum of the main local maxima in $\tilde{\psi}_\perp(\mathbf{k}_\perp)$ with $k_\perp \neq q$ and $k_\perp = q$ equals, i.e., $\sum_{\mathbf{k}_\perp = \mathbf{k}_m} \tilde{\psi}_\perp(\mathbf{k}_\perp)\delta(k_\perp, q) = \sum_{\mathbf{k}_\perp = \mathbf{k}_m} \tilde{\psi}_\perp(\mathbf{k}_\perp)[1 - \delta(k_\perp, q)]$, where $\{\mathbf{k}_m\}$ stand for the set of momenta of the local maxima in $\tilde{\psi}_\perp(\mathbf{k}_\perp)$ and $\delta(a, b)$ corresponds to the Kronecker delta function. As can be observed in Fig. 1, for large enough U_0, the depletion effects on lattice minima produced by the dipolar interaction are always strong enough, avoiding us seeing a transition from SQC_2 to BG_2. Nevertheless, we expect this to be the case for large a_s/a_{dd}, as reported in Ref. [59] for the case of contact-interacting bosons.

Remarkably, we observe the TSS-to-SSS phase transition although the SSS is never the ground state of the system at $U_0 = 0$ for the set of parameters considered [46,47]. Indeed, by increasing U_0 we promote the localization of particles at the minima of the QCL, inducing an increment of the size of the clusters and of the dipolar repulsion between clusters, favoring the transition to the SSS phase. The TSS-to-SSS transition was already observed in the absence of the QCL [46]. In this case, the enlargement of the cluster sizes is achieved by increasing the system density.

The obtained phase diagram can be understood with the help of Fig. 2, where we depict the observed ground-state configurations. For weak QCLs, the ground state corresponds to the TSS state shown in Fig. 2(a). As U_0 is increased, we see a transition to the SSS state, Fig. 2(b). In the intermediate U_0 regime, the stripe ansatz evolves to the SQC_1 state, Fig. 2(c). In Figs. 2(d)–2(f), we show the density patterns along the $y = 0$ line where the enlargement of the TSS cluster triggering the transition to the SSS and SQC_1 states can be observed. To some extent, stabilization of superfluid clusters and stripes is boosted by a process reminiscent of superfluids caged in puddles, as featured in BG phases [52,73–77].

In Fig. 3, we show the behavior of quantities used to characterize the phases of the system and to locate their boundaries in Fig. 1. Additionally, we considered the density contrast to classify solid states [71]. We computed the superfluid fraction considering a generalization of Leggett's criterion [78],

$$f = \frac{L_x^2 L_y^2}{\int d\mathbf{r}_\perp \rho_\perp(\mathbf{r}_\perp) \int d\mathbf{r}_\perp \rho_\perp(\mathbf{r}_\perp)^{-1}}, \qquad (2)$$

where $L_{x(y)}$ is the length of the system in the $x(y)$ direction, see Ref. [13]. At strong U_0, the SQC transitions to the BG whenever $f = 0$. To differentiate between a BG and a Mott insulator, we consider local superfluidity on the first ring of clusters around the origin [71]. Both BG and insulating states have zero global superfluidity, but the former has local superfluidity in some puddles. The local superfluid fraction on a ring of radius R is $f_{\mathrm{loc}} = 4\pi^2 / \int_0^{2\pi} R d\theta \rho_\perp^{-1}(\mathbf{R})$, where $\mathbf{R} = (R\cos\theta, R\sin\theta)$ [79]. In Fig. 3(a), we show the local superfluid fraction and see that it remains finite when the global superfluidity vanishes ($U_0 \gtrsim 1.69$), which indicates that in the strong U_0 regime, the system is a BG.

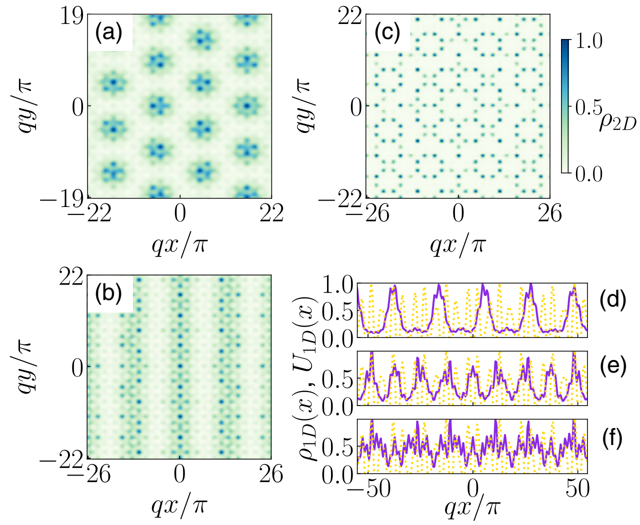

FIG. 2. Normalized density patterns. (a)–(c) Two-dimensional density $\rho_{2D} = \rho_\perp(x, y)/\rho_\perp^{\max}$ obtained via the numerical solution of Eq. (1). (d)–(f) $\rho_{1D}(x) = \rho_\perp(x, 0)/\rho_\perp^{\max}$ (solid curves) and QCL $U_{1D}(x) = U_q(x, 0)/U_q^{\max}$ (dotted curves), at the $y = 0$ line. The system parameters are the same as in Fig. 1 with $a_s/a_{dd} = 0.78$. In (a),(d), the system is in the TSS state with $U_0 = 0.20$. In (b),(e), the SSS state is represented for $U_0 = 0.32$. In (c),(f), the SQC_1 state is shown for $U_0 = 1.44$. The BG_1 state is visually indistinguishable from the SQC_1. See density patterns (a)–(c) amplified in the Supplemental Material [71].

At intermediate U_0, we observe a competition between the SSS (TSS) and QCL patterns. To measure how much each of these patterns contributes to the mixed state, we study the Fourier transform of the density $\tilde{\rho}_\perp(\mathbf{k}_\perp) = \int d\mathbf{r}_\perp \rho_\perp(\mathbf{r}_\perp) e^{-i\mathbf{k}_\perp \cdot \mathbf{r}_\perp}$. The SSS (TSS) and QCL patterns have, respectively, two (six) and eight characteristic peaks in the profile of $\tilde{\rho}_\perp(\mathbf{k}_\perp)$. Once we measure the average height h of each kind of characteristic peaks, see details in Ref. [71], we estimate the SSS (TSS) composition through the parameters $\Delta_{\mathrm{SSS(TSS)}} = h_{\mathrm{SSS(TSS)}}/(h_{\mathrm{SSS(TSS)}} + h_{\mathrm{SQC}})$ and $\Delta_{\mathrm{SQC}} = h_{\mathrm{SQC}}/(h_{\mathrm{SSS(TSS)}} + h_{\mathrm{SQC}})$ [80]. The SSS (TSS) to SQC phase transition is thus identified as the lower bound of a phase in which $\Delta_{\mathrm{SQC}} > \Delta_{\mathrm{SSS(TSS)}}$, see Fig. 3(b).

The phenomenology discussed so far corresponds to a situation in which $q \gg k_0$. The role of q has been grasped

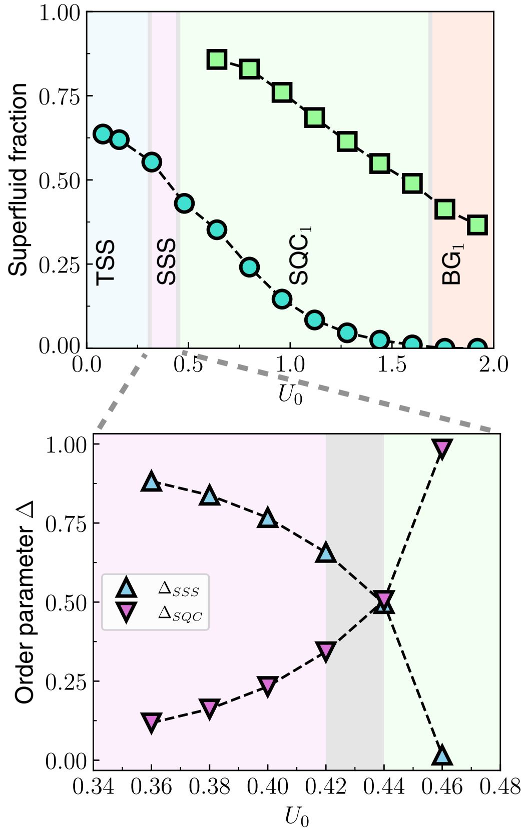

FIG. 3. Characterization of the system ground state. We display the global superfluid fraction (circles), the local superfluid fraction (squares), and the SSS and SQC order parameters, Δ_{SSS} and Δ_{SQC}, respectively. The gray regions delimit the phase transitions. The system parameters are the same as in Fig. 2.

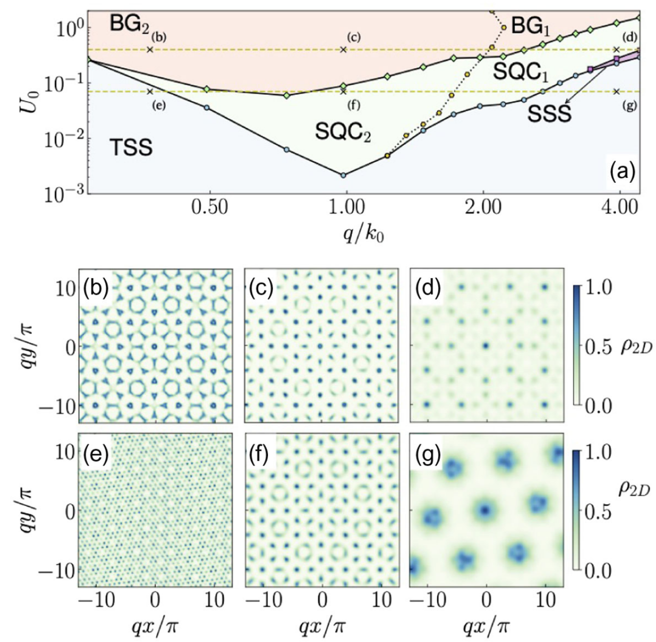

FIG. 4. Phase diagram of dipolar bosons in the q versus U_0 plane. (a) Phase diagram obtained through the SVM at $\bar{\rho}_\perp = 120$ and $a_s/a_{dd} = 0.77$, we indicate with crosses the positions of the density patterns shown in (b)–(g). All the system parameters, but q, are the same as in Fig. 2. (b)–(d) Three density patterns at $U_0 = 0.40$ and (b) $q = 0.15$, (c) $q = 0.4$, and (d) $q = 1.6$. (e)–(g) Three density patterns at $U_0 = 0.07$ and (e) $q = 0.15$, (f) $q = 0.4$, and (g) $q = 1.6$.

by employing the SVM. Figure 4(a) depicts the phase diagram by varying q/k_0 and U_0, keeping both density $\bar{\rho}_\perp$ and a_s/a_{dd} fixed. For $q \lesssim k_0$, the TSS melts into the SQC_2 due to the competition with the QCL ordering for small values of U_0. In this case, the quasicrystalline pattern matches the QCL since the distance between neighboring sites is large enough to hinder the dipolar repulsion. Additionally, we also observe the BG_2 phase matching the lattice. In panels (b)–(g), we show the ground-state configuration as q increases for two different values of U_0. Importantly, we notice the existence of two opposite regimes of the TSS state. For $q \gg k_0$ we observe a triangular arrangement of clusters decorated by the QCL pattern [Fig. 4(g)], while for $q \ll k_0$, the TSS state is structured as a quasicrystalline arrangement of clusters decorated by the triangular modulation [Fig. 4(e)]. For strong U_0, the BG phase surprisingly melts in the superfluid SQC even if increasing q is similar to increasing density. This phenomenology is also observed in contact-interaction systems [59].

Experimental feasibility—The results presented here are in a regime of parameters within current experimental capabilities [37,39,48,81,82]. We propose a potential experiment using ^{162}Dy atoms. This system offers a wide range of s-wave scattering lengths a_s, with a dipolar length $a_{dd} \approx 7$ nm, which results in a range of a_s/a_{dd} consistent with the values considered in this work. For ^{162}Dy, the characteristic units of length and time are $\ell = 0.26$ μm and $t_0 = 0.18$ ms. The trapping dimensionless frequency $\omega_z t_0 = 0.08$ is equivalent to $\omega_z \approx 450$ Hz. For $a_s/a_{dd} = 0.77$ and effective two-dimensional density $\bar{\rho}_\perp = 120$, we estimate a condensate thickness $\sigma_z \approx 7.8$ μm and a peak 3D density in the absence of the QCL $3\rho_\perp/4\sigma_z \approx 1.65 \times 10^{14}$ cm^{-3}. In these conditions, the ground-state characteristic wave vector of the triangular solid is $k_0 \approx 0.4$, resulting in a lattice spacing $\lambda = 4\pi/(\sqrt{3}k_0) \approx 4.7$ μm, a small enough value to experimentally detect the long-distance properties of the predicted phases.

Recent works have successfully replicated the potential of an octagonal QCL using optical lattices [56,57]. The experimental setup involves superimposing four coplanar 1D lattices, formed by retroreflective laser beams, arranged at 45° angles relative to each other. We considered QCLs whose characteristic wave vector q approximately varies in the range from $k_0/4$ to $4k_0$, which results in a wavelength interval $\Delta\lambda_q \approx (1.02, 16.3)$ μm. For the lattice intensity U_0, our theoretical parameters also fall into an experimentally feasible region. In [57], the authors use U_0 values up to

$4.6E_r$ (E_r being the recoil energy), equivalent to $U_0 = 1.27$ in our units. This value falls within the BG phase in Fig. 4.

We have considered finite-temperature corrections to our energy functional perturbatively [83,84]. Our calculations show that the phases observed remain robust for temperatures up to $T \sim 40$ nK (see Supplemental Material [71]). Regarding the effects of quantum fluctuations, it is known that the GPE description fails in the dilute regime [85]. Nonetheless, for the regime of parameters explored, corresponding to the high-density supersolid phase at $U_0 = 0$, we expect weak quantum correlations, therefore a valid GPE description. Moreover, the agreement between GPE calculations, quantum Monte Carlo, and experiments has been attested in related scenarios [8,45,86].

Conclusions—In this work, we studied the effects of a QCL on the TSS phase exhibited by a planar system of dipolar bosons near the critical point. For weak QCL with high characteristic momentum, the system develops a triangular or stripe pattern decorated with a quasicrystalline structure that exhibits global superfluid properties. Interestingly, we observe that the TSS-to-SSS transition increasing the depth of the QCL occurs as a mechanism to minimize the dipolar repulsion when $q \gg k_0$. A further increase of U_0 at the TSS or SSS phases eventually triggers a transition to the SQC phase and later to the BG phase. Moreover, by enlarging q, we observe that the quasicrystal phases develop a crossover from a state where the density pattern matches the QCL to a state in which they are different. Finally, the insights from our investigation have laid the foundation for the experimental exploration, enabling us to understand the physics of long-range interacting quantum gases in quasiperiodic geometries.

Acknowledgments—We acknowledge M. Ciardi and Y.-C. Zhang for useful discussions. F. C. and V. Z. acknowledge financial support from PNRR MUR (Piano Nazionale di Ripresa e Resilienza/Ministero dell'Università e della Ricerca) Project No. PE0000023-NQSTI. V. Z. thanks the Instituto Serrapilheira for its support (Grant Number Serra-1812-27802). A. M. C. acknowledges MPIPKS (Max Planck Institut für Physik Komplexer Systeme) for financial support and hospitality. We thank the High-Performance Computing Center (NPAD) at UFRN (Universidade Federal do Rio Grande do Norte) and the NICIS (National Integrated Cyber Infrastructure System) Centre for High-Performance Computing, South Africa, for providing computational resources within the program PHYS0892.

[1] Nicolò Defenu, Tobias Donner, Tommaso Macrì, Guido Pagano, Stefano Ruffo, and Andrea Trombettoni, Long-range interacting quantum systems, Rev. Mod. Phys. **95**, 035002 (2023).

[2] S. A. Kivelson, E. Fradkin, and V. J. Emery, Electronic liquid-crystal phases of a doped Mott insulator, Nature (London) **393**, 550 (1998).

[3] R. M. Fernandes, A. V. Chubukov, and J. Schmalian, What drives nematic order in iron-based superconductors?, Nat. Phys. **10**, 97 (2014).

[4] Rong Yu, Liang Yin, Neil S. Sullivan, J. S. Xia, Chao Huan, Armando Paduan-Filho, Nei F. Oliveira Jr, Stephan Haas, Alexander Steppke, Corneliu F. Miclea, Franziska Weickert, Roman Movshovich, Eun-Deok Mun, Brian L. Scott, Vivien S. Zapf, and Tommaso Roscilde, Bose glass and Mott glass of quasiparticles in a doped quantum magnet, Nature (London) **489**, 379 (2012).

[5] Jr-Chiun Yu, Shaurya Bhave, Lee Reeve, Bo Song, and Ulrich Schneider, Observing the two-dimensional Bose glass in an optical quasicrystal, arXiv:2303.00737.

[6] Massimo Boninsegni and Nikolay V. Prokof'ev, Colloquium: Supersolids: What and where are they?, Rev. Mod. Phys. **84**, 759 (2012).

[7] T. Macrì, F. Maucher, F. Cinti, and T. Pohl, Elementary excitations of ultracold soft-core bosons across the superfluid-supersolid phase transition, Phys. Rev. A **87**, 061602(R) (2013).

[8] F. Cinti, T. Macrì, W. Lechner, G. Pupillo, and T. Pohl, Defect-induced supersolidity with soft-core bosons, Nat. Commun. **5**, 3235 (2014).

[9] Alessio Recati and Sandro Stringari, Supersolidity in ultracold dipolar gases, Nat. Rev. Phys. **5**, 735 (2023).

[10] Sarang Gopalakrishnan, Ivar Martin, and Eugene A. Demler, Quantum quasicrystals of spin-orbit-coupled dipolar bosons, Phys. Rev. Lett. **111**, 185304 (2013).

[11] Matteo Ciardi, Adriano Angelone, Fabio Mezzacapo, and Fabio Cinti, Quasicrystalline Bose glass in the absence of disorder and quasidisorder, Phys. Rev. Lett. **131**, 173402 (2023).

[12] Guido Pupillo, Primož Ziherl, and Fabio Cinti, Quantum cluster quasicrystals, Phys. Rev. B **101**, 134522 (2020).

[13] A. Mendoza-Coto, R. Turcati, V. Zampronio, R. Díaz-Méndez, T. Macrì, and F. Cinti, Exploring quantum quasicrystal patterns: A variational study, Phys. Rev. B **105**, 134521 (2022).

[14] Matheus Grossklags, Matteo Ciardi, Vinicius Zampronio, Fabio Cinti, and Alejandro Mendoza-Coto, Self-induced Bose glass phase in quantum cluster quasicrystals, arXiv:2308.12434.

[15] D. Jaksch and P. Zoller, The cold atom Hubbard toolbox, Ann. Phys. (Amsterdam) **315**, 52 (2005), special Issue.

[16] Andrew J. Daley, Quantum computing and quantum simulation with group-II atoms, Quantum Inf. Process. **10**, 865 (2011).

[17] Daniel González-Cuadra, Przemysław R. Grzybowski, Alexandre Dauphin, and Maciej Lewenstein, Strongly correlated bosons on a dynamical lattice, Phys. Rev. Lett. **121**, 090402 (2018).

[18] Florian Schäfer, Takeshi Fukuhara, Seiji Sugawa, Yosuke Takasu, and Yoshiro Takahashi, Tools for quantum simulation with ultracold atoms in optical lattices, Nat. Rev. Phys. **2**, 411 (2020).

[19] Fabio Cinti, Massimo Boninsegni, and Thomas Pohl, Exchange-induced crystallization of soft-core bosons, New J. Phys. **16**, 033038 (2014).

[20] F. Wächtler and L. Santos, Quantum filaments in dipolar Bose-Einstein condensates, Phys. Rev. A **93**, 061603(R) (2016).

[21] F. Wächtler and L. Santos, Ground-state properties and elementary excitations of quantum droplets in dipolar Bose-Einstein condensates, Phys. Rev. A **94**, 043618 (2016).

[22] T. Lahaye, C. Menotti, L. Santos, M. Lewenstein, and T. Pfau, The physics of dipolar bosonic quantum gases, Rep. Prog. Phys. **72**, 126401 (2009).

[23] Zhen-Kai Lu, Yun Li, D. S. Petrov, and G. V. Shlyapnikov, Stable dilute supersolid of two-dimensional dipolar bosons, Phys. Rev. Lett. **115**, 075303 (2015).

[24] D. Baillie and P. B. Blakie, Droplet crystal ground states of a dipolar Bose gas, Phys. Rev. Lett. **121**, 195301 (2018).

[25] Hiroki Saito, Path-integral Monte Carlo study on a droplet of a dipolar Bose-Einstein condensate stabilized by quantum fluctuation, J. Phys. Soc. Jpn. **85**, 053001 (2016).

[26] F. Cinti, P. Jain, M. Boninsegni, A. Micheli, P. Zoller, and G. Pupillo, Supersolid droplet crystal in a dipole-blockaded gas, Phys. Rev. Lett. **105**, 135301 (2010).

[27] Kwangsik Nho and D. P. Landau, Bose-Einstein condensation of trapped atoms with dipole interactions, Phys. Rev. A **72**, 023615 (2005).

[28] Fabio Cinti and Massimo Boninsegni, Classical and quantum filaments in the ground state of trapped dipolar Bose gases, Phys. Rev. A **96**, 013627 (2017).

[29] Youssef Kora and Massimo Boninsegni, Patterned supersolids in dipolar Bose systems, J. Low Temp. Phys. **197**, 337 (2019).

[30] Fabio Cinti, Alberto Cappellaro, Luca Salasnich, and Tommaso Macrì, Superfluid filaments of dipolar bosons in free space, Phys. Rev. Lett. **119**, 215302 (2017).

[31] Yong-Chang Zhang, Fabian Maucher, and Thomas Pohl, Supersolidity around a critical point in dipolar Bose-Einstein condensates, Phys. Rev. Lett. **123**, 015301 (2019).

[32] Santo Maria Roccuzzo and Francesco Ancilotto, Supersolid behavior of a dipolar Bose-Einstein condensate confined in a tube, Phys. Rev. A **99**, 041601(R) (2019).

[33] Eli J. Halperin, Shai Ronen, and J. L. Bohn, Frustration in a dipolar Bose-Einstein condensate introduced by an optical lattice, Phys. Rev. A **107**, L041301 (2023).

[34] Matteo Ciardi, Fabio Cinti, Giuseppe Pellicane, and Santi Prestipino, Supersolid phases of bosonic particles in a bubble trap, Phys. Rev. Lett. **132**, 026001 (2024).

[35] Jun-Ru Li, Jeongwon Lee, Wujie Huang, Sean Burchesky, Boris Shteynas, Furkan Çağrı Top, Alan O. Jamison, and Wolfgang Ketterle, A stripe phase with supersolid properties in spin–orbit-coupled Bose-Einstein condensates, Nature (London) **543**, 91 (2017).

[36] Julian Léonard, Andrea Morales, Philip Zupancic, Tilman Esslinger, and Tobias Donner, Supersolid formation in a quantum gas breaking a continuous translational symmetry, Nature (London) **543**, 87 (2017).

[37] L. Tanzi, E. Lucioni, F. Famà, J. Catani, A. Fioretti, C. Gabbanini, R. N. Bisset, L. Santos, and G. Modugno, Observation of a dipolar quantum gas with metastable supersolid properties, Phys. Rev. Lett. **122**, 130405 (2019).

[38] L. Tanzi, S. M. Roccuzzo, E. Lucioni, F. Famà, A. Fioretti, C. Gabbanini, G. Modugno, A. Recati, and S. Stringari, Supersolid symmetry breaking from compressional oscillations in a dipolar quantum gas, Nature (London) **574**, 382 (2019).

[39] Fabian Böttcher, Jan-Niklas Schmidt, Matthias Wenzel, Jens Hertkorn, Mingyang Guo, Tim Langen, and Tilman Pfau, Transient supersolid properties in an array of dipolar quantum droplets, Phys. Rev. X **9**, 011051 (2019).

[40] L. Chomaz, D. Petter, P. Ilzhöfer, G. Natale, A. Trautmann, C. Politi, G. Durastante, R. M. W. van Bijnen, A. Patscheider, M. Sohmen, M. J. Mark, and F. Ferlaino, Long-lived and transient supersolid behaviors in dipolar quantum gases, Phys. Rev. X **9**, 021012 (2019).

[41] Mingyang Guo, Fabian Böttcher, Jens Hertkorn, Jan-Niklas Schmidt, Matthias Wenzel, Hans Peter Büchler, Tim Langen, and Tilman Pfau, The low-energy Goldstone mode in a trapped dipolar supersolid, Nature (London) **574**, 386 (2019).

[42] G. Natale, R. M. W. van Bijnen, A. Patscheider, D. Petter, M. J. Mark, L. Chomaz, and F. Ferlaino, Excitation spectrum of a trapped dipolar supersolid and its experimental evidence, Phys. Rev. Lett. **123**, 050402 (2019).

[43] Matthew A. Norcia, Claudia Politi, Lauritz Klaus, Elena Poli, Maximilian Sohmen, Manfred J. Mark, Russell N. Bisset, Luis Santos, and Francesca Ferlaino, Two-dimensional supersolidity in a dipolar quantum gas, Nature (London) **596**, 357 (2021).

[44] Lauriane Chomaz, Igor Ferrier-Barbut, Francesca Ferlaino, Bruno Laburthe-Tolra, Benjamin L. Lev, and Tilman Pfau, Dipolar physics: A review of experiments with magnetic quantum gases, Rep. Prog. Phys. **86**, 026401 (2022).

[45] G. Biagioni, N. Antolini, B. Donelli, L. Pezzè, A. Smerzi, M. Fattori, A. Fioretti, C. Gabbanini, M. Inguscio, L. Tanzi, and G. Modugno, Measurement of the superfluid fraction of a supersolid by Josephson effect, Nature (London) **629**, 773 (2024).

[46] B. T. E. Ripley, D. Baillie, and P. B. Blakie, Two-dimensional supersolidity in a planar dipolar Bose gas, Phys. Rev. A **108**, 053321 (2023).

[47] Yong-Chang Zhang, Thomas Pohl, and Fabian Maucher, Metastable patterns in one- and two-component dipolar Bose-Einstein condensates, Phys. Rev. Res. **6**, 023023 (2024).

[48] Holger Kadau, Matthias Schmitt, Matthias Wenzel, Clarissa Wink, Thomas Maier, Igor Ferrier-Barbut, and Tilman Pfau, Observing the Rosensweig instability of a quantum ferrofluid, Nature (London) **530**, 194 (2016).

[49] P. W. Anderson, Absence of diffusion in certain random lattices, Phys. Rev. **109**, 1492 (1958).

[50] Giacomo Roati, Chiara D'Errico, Leonardo Fallani, Marco Fattori, Chiara Fort, Matteo Zaccanti, Giovanni Modugno, Michele Modugno, and Massimo Inguscio, Anderson localization of a non-interacting Bose–Einstein condensate, Nature (London) **453**, 895 (2008).

[51] Giovanni Modugno, Anderson localization in Bose–Einstein condensates, Rep. Prog. Phys. **73**, 102401 (2010).

[52] Matthew P. A. Fisher, Peter B. Weichman, G. Grinstein, and Daniel S. Fisher, Boson localization and the superfluid-insulator transition, Phys. Rev. B **40**, 546 (1989).

[53] Dmitry A. Abanin, Ehud Altman, Immanuel Bloch, and Maksym Serbyn, Colloquium: Many-body localization, thermalization, and entanglement, Rev. Mod. Phys. **91**, 021001 (2019).

[54] Attila Szabó and Ulrich Schneider, Mixed spectra and partially extended states in a two-dimensional quasiperiodic model, Phys. Rev. B **101**, 014205 (2020).

[55] Hepeng Yao, Alice Khoudli, Léa Bresque, and Laurent Sanchez-Palencia, Critical behavior and fractality in shallow one-dimensional quasiperiodic potentials, Phys. Rev. Lett. **123**, 070405 (2019).

[56] Konrad Viebahn, Matteo Sbroscia, Edward Carter, Jr-Chiun Yu, and Ulrich Schneider, Matter-wave diffraction from a quasicrystalline optical lattice, Phys. Rev. Lett. **122**, 110404 (2019).

[57] Matteo Sbroscia, Konrad Viebahn, Edward Carter, Jr-Chiun Yu, Alexander Gaunt, and Ulrich Schneider, Observing localization in a 2d quasicrystalline optical lattice, Phys. Rev. Lett. **125**, 200604 (2020).

[58] Hepeng Yao, Thierry Giamarchi, and Laurent Sanchez-Palencia, Lieb-Liniger bosons in a shallow quasiperiodic potential: Bose glass phase and fractal Mott lobes, Phys. Rev. Lett. **125**, 060401 (2020).

[59] Ronan Gautier, Hepeng Yao, and Laurent Sanchez-Palencia, Strongly interacting bosons in a two-dimensional quasicrystal lattice, Phys. Rev. Lett. **126**, 110401 (2021).

[60] Matteo Ciardi, Tommaso Macrì, and Fabio Cinti, Finite-temperature phases of trapped bosons in a two-dimensional quasiperiodic potential, Phys. Rev. A **105**, L011301 (2022).

[61] Zhaoxuan Zhu, Shengjie Yu, Dean Johnstone, and Laurent Sanchez-Palencia, Localization and spectral structure in two-dimensional quasicrystal potentials, Phys. Rev. A **109**, 013314 (2024).

[62] Zhaoxuan Zhu, Hepeng Yao, and Laurent Sanchez-Palencia, Thermodynamic phase diagram of two-dimensional bosons in a quasicrystal potential, Phys. Rev. Lett. **130**, 220402 (2023).

[63] Franco Dalfovo, Stefano Giorgini, Lev P. Pitaevskii, and Sandro Stringari, Theory of Bose-Einstein condensation in trapped gases, Rev. Mod. Phys. **71**, 463 (1999).

[64] Anthony J. Leggett, Bose-Einstein condensation in the alkali gases: Some fundamental concepts, Rev. Mod. Phys. **73**, 307 (2001).

[65] It is important to notice that due to the presence of the non-local dipolar interaction, different values of the characteristic wave vector q can produce different many-body ground-state phases.

[66] T. D. Lee, Kerson Huang, and C. N. Yang, Eigenvalues and eigenfunctions of a Bose system of hard spheres and its low-temperature properties, Phys. Rev. **106**, 1135 (1957).

[67] T. D. Lee and C. N. Yang, Many-body problem in quantum mechanics and quantum statistical mechanics, Phys. Rev. **105**, 1119 (1957).

[68] D. S. Petrov, Quantum mechanical stabilization of a collapsing Bose-Bose mixture, Phys. Rev. Lett. **115**, 155302 (2015).

[69] Ralf Schützhold, Michael Uhlmann, Yan Xu, and Uwe R. Fischer, Mean-field expansion in Bose–Einstein condensates with finite-range interactions, Int. J. Mod. Phys. B **20**, 3555 (2006).

[70] R. N. Bisset, R. M. Wilson, D. Baillie, and P. B. Blakie, Ground-state phase diagram of a dipolar condensate with quantum fluctuations, Phys. Rev. A **94**, 033619 (2016).

[71] See Supplemental Material at http://link.aps.org/supplemental/10.1103/PhysRevLett.133.196001 for exploring supersolid phases in dipolar quantum gases through quasicrystalline confinement.

[72] Matheus Grossklags, Matteo Ciardi, Vinicius Zampronio, Fabio Cinti, and Alejandro Mendoza-Coto, Self-induced Bose glass phase in quantum cluster quasicrystals, arXiv:2308.12434.

[73] L. Pollet, N. V. Prokof'ev, B. V. Svistunov, and M. Troyer, Absence of a direct superfluid to Mott insulator transition in disordered Bose systems, Phys. Rev. Lett. **103**, 140402 (2009).

[74] Giuseppe Carleo, Guilhem Boéris, Markus Holzmann, and Laurent Sanchez-Palencia, Universal superfluid transition and transport properties of two-dimensional dirty bosons, Phys. Rev. Lett. **111**, 050406 (2013).

[75] Ş G. Söyler, M. Kiselev, N. V. Prokof'ev, and B. V. Svistunov, Phase diagram of the commensurate two-dimensional disordered Bose-Hubbard model, Phys. Rev. Lett. **107**, 185301 (2011).

[76] Matteo Ciardi, Adriano Angelone, Fabio Mezzacapo, and Fabio Cinti, Quasicrystalline Bose glass in the absence of disorder and quasidisorder, Phys. Rev. Lett. **131**, 173402 (2023).

[77] Bruno R. de Abreu, Fabio Cinti, and Tommaso Macrì, Superstripes and quasicrystals in bosonic systems with hard-soft corona interactions, Phys. Rev. B **105**, 094505 (2022).

[78] A. J. Leggett, Can a solid be "superfluid"?, Phys. Rev. Lett. **25**, 1543 (1970).

[79] Koichiro Furutani and Luca Salasnich, Superfluid properties of bright solitons in a ring, Phys. Rev. A **105**, 033320 (2022).

[80] P. M. Chaikin and T. C. Lubensky, *Principles of Condensed Matter Physics* (Cambridge University Press, Cambridge, England, 1995).

[81] L. Chomaz, R. M. W. van Bijnen, D. Petter, G. Faraoni, S. Baier, J. H. Becher, M. J. Mark, F. Wächtler, L. Santos, and F. Ferlaino, Observation of roton mode population in a dipolar quantum gas, Nat. Phys. **14**, 442 (2018).

[82] Matthias Schmitt, Matthias Wenzel, Fabian Böttcher, Igor Ferrier-Barbut, and Tilman Pfau, Self-bound droplets of a dilute magnetic quantum liquid, Nature (London) **539**, 259 (2016).

[83] J. Sánchez-Baena, C. Politi, F. Maucher, F. Ferlaino, and T. Pohl, Heating a dipolar quantum fluid into a solid, Nat. Commun. **14**, 1868 (2023).

[84] Juan Sánchez-Baena, Thomas Pohl, and Fabian Maucher, Superfluid-supersolid phase transition of elongated dipolar Bose-Einstein condensates at finite temperatures, Phys. Rev. Res. **6**, 023183 (2024).

[85] Fabian Böttcher, Matthias Wenzel, Jan-Niklas Schmidt, Mingyang Guo, Tim Langen, Igor Ferrier-Barbut, Tilman Pfau, Raúl Bombín, Joan Sánchez-Baena, Jordi Boronat, and Ferran Mazzanti, Dilute dipolar quantum droplets beyond the extended Gross-Pitaevskii equation, Phys. Rev. Res. **1**, 033088 (2019).

[86] Hiroki Saito, Path-integral Monte Carlo study on a droplet of a dipolar Bose–Einstein condensate stabilized by quantum fluctuation, J. Phys. Soc. Jpn. **85**, 053001 (2016).